A photoswitchable orange-to-far-red fluorescent protein, PSmOrange

Oksana M Subach[1], George H Patterson[2], Li-Min Ting[3], Yarong Wang[1], John S Condeelis[1] & Vladislav V Verkhusha[1]

We report a photoswitchable monomeric Orange (PSmOrange) protein that is initially orange (excitation, 548 nm; emission, 565 nm) but becomes far-red (excitation, 636 nm; emission, 662 nm) after irradiation with blue-green light. Compared to its parental orange proteins, PSmOrange has greater brightness, faster maturation, higher photoconversion contrast and better photostability. The red-shifted spectra of both forms of PSmOrange enable its simultaneous use with cyan-to-green photoswitchable proteins to study four intracellular populations. Photoconverted PSmOrange has, to our knowledge, the most far-red excitation peak of all GFP-like fluorescent proteins, provides diffraction-limited and super-resolution imaging in the far-red light range, is optimally excited with common red lasers, and can be photoconverted subcutaneously in a mouse. PSmOrange photoswitching occurs via a two-step photo-oxidation process, which causes cleavage of the polypeptide backbone. The far-red fluorescence of photoconverted PSmOrange results from a new chromophore containing *N*-acylimine with a co-planar carbon-oxygen double bond.

Photoconvertible fluorescent proteins are widely used to optically highlight spatiotemporal dynamics of intracellular molecules, organelles and whole cells[1]. There are two types of irreversibly photoconvertible fluorescent proteins: photoactivatable and photoswitchable. Photoactivatable fluorescent proteins (PAFPs) are activated from a non-fluorescent (dark) state to a fluorescent state. This group includes photoactivatable GFP (PAGFP)[2], photoactivatable monomeric Cherry (PAmCherry)[3] and PATagRFP[4]. Photoswitchable fluorescent proteins (PSFPs) switch between two different fluorescent colors. Most PSFPs, including Dendra2 (ref. 5), mEos2 (ref. 6), Kaede[7], KikGR[8], ClavGR2 (ref. 9) and their derivatives, change color from green to red. The only available non-red PSFP is the cyan-to-green PSCFP2 protein[5]. Most photoconvertible fluorescent proteins require irradiation with UV–violet light to become photoconverted. Dendra2 can be also photoconverted with blue light, but this is less effective and requires high-intensity illumination[5].

Several super-resolution microscopy techniques, such as photoactivated localization microscopy (PALM)[10] and stochastic optical reconstruction microscopy[10], use photoactivatable or photoswitchable fluorophores. PALM techniques use both PAFPs and PSFPs. Super-resolution techniques can also use reversibly switchable fluorescent proteins in PALM with independently running acquisition (PALMIRA) mode[11] and conventional fluorescent proteins in ground state depletion-individual molecule return (GSDIM) mode[12]. Multicolor PALM provides information about the spatial and temporal heterogeneity of several types of molecules in a cell, but compatible photoconvertible fluorescent proteins are currently limited to green and red[3,4]. Adding a third color would be beneficial because the relative intracellular localization of three proteins can then be compared directly, and cell-to-cell variability is less of a problem.

Noninvasive imaging of animals requires the development of genetically encoded fluorescent probes with excitation and emission spectra in the near-infrared region, which has the lowest hemoglobin, melanin and water absorbance[13]. The tissue absorbance in this optical window drops so substantially that even dim far-red fluorescent proteins perform better than bright green fluorescent proteins[14]. There are several conventional far-red fluorescent proteins with excitation and emission maxima up to 611 nm and 670 nm, respectively[15–19]. However, there is a limited number of far-red PAFPs and PSFPs.

It has been shown that a conventional fluorescent protein mOrange photoconverts to a far-red form after irradiation of the orange form with 458 nm or 488 nm light[20]. However, low photostability and low far-red brightness limit the use of mOrange as a photoswitchable tag. An aerobic effect, called photo-oxidative redding, occurs in green fluorescent proteins of different origins in the presence of oxidants[21]. Notably, photobleaching of mOrange occurs substantially faster in the presence of oxygen than in oxygen-free conditions[22] suggesting that mOrange photoconversion may be affected by intracellular oxidants.

It would advance various imaging techniques to have a PSFP that is photoswitchable with visible light, exhibits fluorescent colors distinct from those of existing PSFPs, has far-red photoswitched color for deep-tissue imaging and is optimized for the redox conditions of live cells. In this work we explored the ability

[1]Department of Anatomy and Structural Biology, and Gruss-Lipper Biophotonics Center, Albert Einstein College of Medicine, Bronx, New York, USA. [2]Biophotonics Section, National Institute of Biomedical Imaging and Bioengineering, National Institutes of Health, Bethesda, Maryland, USA. [3]Department of Immunology and Microbiology, and Department of Medicine, Albert Einstein College of Medicine, Bronx, New York, USA. Correspondence should be addressed to V.V.V. (vladislav.verkhusha@einstein.yu.edu).

RECEIVED 7 DECEMBER 2010; ACCEPTED 29 JUNE 2011; PUBLISHED ONLINE 31 JULY 2011; DOI:10.1038/NMETH.1664

Table 1 | Properties of the orange and far-red forms of purified proteins

	mOrange		mOrange2		PSmOrange	
	Orange form	Far-red form	Orange form	Far-red form	Orange form	Far-red form
Absorbance/excitation (nm)	546	631	549	632	548	634/636
Emission (nm)	562	662	565	663	565	662
Extinction coefficient (M^{-1} cm^{-1})	71,000	17,200	58,000[a]	ND	113,300	32,700
Quantum yield	0.69[a]	0.19	0.6[a]	ND	0.51	0.28
Brightness relative to EGFP (%)	148	10	105	ND	176	28
Photoswitching $t_{0.5}$ ± s.d. (s)[b]	12 ± 6		8.0 ± 0.4		15 ± 3	
Far-red increase (fold)	190		240		560	
Photoswitching contrast ± s.d. (fold)[c]	2,800 ± 200		ND		10,700 ± 500	
Photobleaching $t_{0.5}$ ± s.d. (s)[d]	0.65 ± 0.39	17.0 ± 3.7	7 ± 3	ND	15 ± 5	48.5 ± 8.2
pK_a ± s.d.[e]	6.5[a]	ND	6.5[a]	ND	6.2 ± 0.1	5.6 ± 0.1
Maturation half-time at 37 °C (h)	2.5		4.5[a]		1.6	

ND, not determined.

[a]Data were obtained from ref. 22. [b]Determined at 1,050 W cm^{-2} at the sample (n = 10). [c]Determined as the product of the far-red fluorescence increase and the orange fluorescence decrease after photoswitching (n = 3). [d]Determined at 1,130 W cm^{-2} at the sample for the orange form and at 870 W cm^{-2} at the sample for the far-red form (n = 5). [e]n = 4.

of mOrange to photoswitch into the far-red form and the effect of oxidant agents on fluorescent-protein photoconversion. We developed a bright monomeric orange probe with high-contrast photoswitching from orange to far-red.

RESULTS

Development of photoswitchable orange fluorescent protein

We used the *mOrange* gene as a template to develop an mOrange variant that photoswitches from orange to far-red. First we introduced mutations resulting in Q63H and F100Y substitutions (numbering is based on alignment with enhanced GFP (EGFP)), responsible for high photostability of mOrange2 (ref. 22). We subjected the resulting *mOrange(Q63H,F100Y)* gene to nine rounds of random mutagenesis using error-prone PCR. We selected a gene encoding the mOrange(S21T,H63L,F100Y,L125M,K166R, P192S) variant and named it photoswitchable monomeric Orange (PSmOrange) (**Supplementary Fig. 1**). Before photoswitching, PSmOrange exhibited orange fluorescence with excitation and emission peaks at 548 nm and 565 nm, respectively (**Table 1**). After photoswitching with blue-green light, it showed far-red fluorescence with excitation and emission maxima at 636 nm and 662 nm, respectively (**Fig. 1a**). Irradiation with violet light resulted in 6% of the rate of PSmOrange photoswitching and in 14% of the maximal far-red fluorescence relative to that obtained after irradiation with blue light of the same intensity (**Supplementary Fig. 2a**,**b**).

Properties of PSmOrange

When expressed in mammalian cells, PSmOrange and other mutants we obtained had faster kinetics of photoswitching than the purified proteins, suggesting that the intracellular redox environment might affect the process. Therefore, we examined the effect of oxidants on the PSmOrange purified protein. It has been shown that potassium ferricyanide, $K_3Fe(CN)_6$, performed as an optimal model oxidant in the oxidative redding of various green fluorescent proteins *in vitro*, mimicking their photoswitching in mammalian cells[21]. We observed that brightness and photostability of the PSmOrange far-red form was almost independent of $K_3Fe(CN)_6$ concentration over a wide range (**Fig. 1b**) but that higher oxidant concentrations substantially decreased the PSmOrange photoswitching half-time (**Fig. 1c**). The photoswitching half-time of PSmOrange in live mammalian cells corresponded to that observed with the purified protein at $K_3Fe(CN)_6$ concentration of 0.25 mM (**Fig. 1d**). To match the effect of intracellular redox agents on PSmOrange behavior, we characterized purified PSmOrange in the presence of 0.25 mM $K_3Fe(CN)_6$. At high intensity of photoswitching light, PSmOrange exhibited a 1.25-fold longer photoswitching half-time compared to mOrange (**Fig. 1e**,**f**). The photoswitching half-time of mOrange2 was even shorter than that of mOrange, and its maximal far-red fluorescence was 16% and 42% compared to PSmOrange and mOrange, respectively. The far-red form was generated with mono-exponential kinetics, whereas switching off kinetics of the orange form was bi-exponential, suggesting that switching off is a complex photochemical process involving at least two pathways, of which the photoconversion is a major one.

The initial rate of PSmOrange photoswitching using both blue and green light depended on the light intensity in a nonlinear fashion (**Supplementary Fig. 2c**,**d**). On the logarithmic scale, the initial rate had a linear dependence on light intensity with a slope of 2.01 (**Fig. 1g**), suggesting that PSmOrange photoswitching required two photons. We concluded that PSmOrange photoswitching is a two-step photochemical process.

Compared to parental mOrange, PSmOrange was 1.2-fold brighter in the orange state and 2.8-fold brighter in the far-red state (**Table 1**). The photoswitching orange to far-red fluorescence contrast achieved with purified PSmOrange protein was ~4-fold higher than for mOrange. PSmOrange had p*K*a values of 6.2 and 5.6 before and after photoswitching, respectively (**Supplementary Fig. 3a**). Maturation of PSmOrange at 37 °C was 1.6-fold faster compared to mOrange (**Supplementary Fig. 3b**). Similarly to mOrange and mEGFP, purified PSmOrange exhibited monomeric behavior (**Supplementary Fig. 4**).

At high light intensity, photobleaching of the orange and far-red fluorescence signals of PSmOrange was 4% and 35% compared to parental mOrange (**Supplementary Fig. 3c**), although this difference in photostability decreased with decreasing power of the photobleaching light (**Fig. 1h**,**i**). The orange form of PSmOrange was about twofold more photostable than that of mOrange2 at high light intensity and had the same photostability at low light intensity (**Fig. 1h**). We did not study the photostability of the mOrange2 far-red form because of inefficient mOrange2 photoswitching (**Fig. 1f**).

We calculated the fluorescence brightness of the far-red form of PSmOrange above 650 nm at 633 nm excitation as a criterion

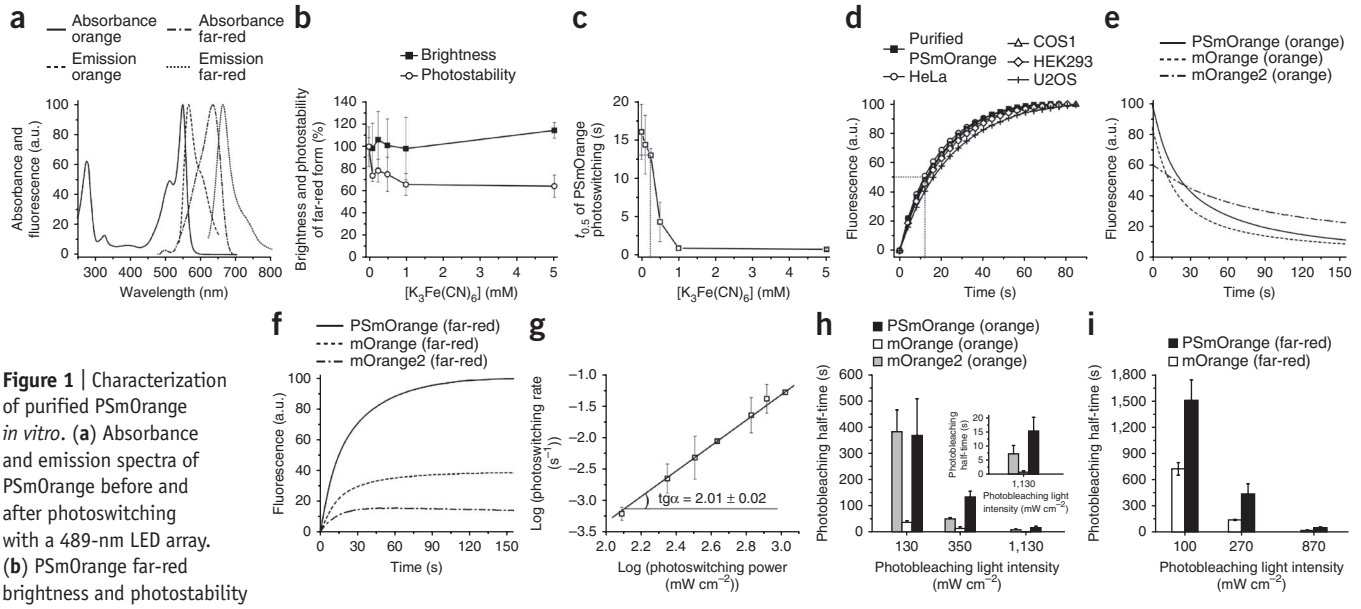

Figure 1 | Characterization of purified PSmOrange *in vitro*. (**a**) Absorbance and emission spectra of PSmOrange before and after photoswitching with a 489-nm LED array. (**b**) PSmOrange far-red brightness and photostability in the presence of indicated amounts of $K_3Fe(CN)_6$ concentrations. (**c**) Photoswitching half-times ($t_{0.5}$) for PSmOrange at indicated $K_3Fe(CN)_6$ concentrations. Half-time at 0.25 mM oxidant is shown by dotted line. (**d**) Formation of the far-red form over time for purified PSmOrange (in 0.25 mM $K_3Fe(CN)_6$) and for cytoplasmic PSmOrange inside the indicated mammalian cells. The half-time for the purified protein is indicated by dotted line. (**e**–**f**) Photoswitching kinetics for orange (**e**) and far-red (**f**) forms of the indicated proteins. (**g**) PSmOrange initial photoswitching rate at indicated power values of the photoswitching 480/40 nm light. (**h**,**i**) Photobleaching half-times for the orange (**h**) and far-red (**i**) forms of the indicated fluorescent proteins at indicated power densities. Inset, magnification of data for 1,130 mW cm^{-2} power. The power densities were estimated at the sample. The photobleaching data (**h**,**i**) were normalized to the spectral output of the lamp, transmission profile of the filter and dichroic mirror and absorbance spectra of the proteins. Error bars, s.d.; $n = 10$ (**b**,**c**) and $n = 5$ (**g**–**i**).

for practical application with common HeNe and red diode lasers[15,17,18]. The brightness of photoswitched PSmOrange in the far-red region was about sixfold greater than that of the most far-red shifted fluorescent proteins, such as mNeptune[18], TagRFP657 (ref. 15) and eqFP670 (ref. 19) (**Supplementary Table 1**). We also compared PSmOrange and several far-red fluorescent proteins expressed in bacterial cells, using a FACS machine equipped with a standard 638-nm excitation laser and a 660/20 nm emission filter. The mean fluorescence brightness of cells with the photoswitched PSmOrange was substantially higher than that of cells expressing the other fluorescent proteins (**Supplementary Fig. 5**).

Behavior of PSmOrange in live mammalian cells

We fused PSmOrange to several cellular proteins and examined expression patterns in HeLa cells. PSmOrange fusions with α-tubulin, vimentin, keratin, paxillin, myosin and histone H2B localized properly in live cells and did not affect cell division (**Supplementary Fig. 6**).

It has been shown that some fluorescent proteins are cytotoxic when expressed at high concentrations using transient expression[23]. We compared cytotoxicity of PSmOrange with that of mEGFP as a non-cytotoxic control[23] using transient transfection of HeLa cells (**Supplementary Fig. 7a**). Relative changes in mean fluorescence intensity of the PSmOrange-expressing cells over time were similar to those of the mEGFP-expressing cells. Next, to test PSmOrange cytotoxicity over longer periods, we made stable preclonal mixtures of MTLn3 cells expressing PSmOrange, mEGFP or mKate2 (ref. 17). We collected the brightest fluorescent cell population for each reporter by FACS 18 d after transfection (**Supplementary Fig. 7b**), cultured them for 19 more days and then analyzed them by FACS. Mean fluorescence intensities of PSmOrange- and mEGFP-expressing cells changed slightly after 19 d of culture, whereas culture of mKate2-expressing cells had many cells with decreased mean fluorescence. Lastly, we tested whether PSmOrange is cytotoxic in a mouse. We injected PSmOrange- or GFP-expressing MTLn3 cells into mouse mammary glands and observed tumor growth by monitoring orange and green fluorescence over time (**Supplementary Fig. 7c**). Fluorescence of the GFP-expressing tumor reached a plateau after 33 d, whereas fluorescence of the PSmOrange-expressing tumor increased up to 46 d. These data demonstrate that PSmOrange has similar cytotoxicity to mEGFP or GFP.

The red-shifted spectra of both forms of PSmOrange, as compared to other red PSFPs, could allow for the simultaneous intracellular use of PSmOrange with the photoswitchable cyan-to-green PSCFP2. To test this, we expressed nuclear localization signal (NLS)-PSCFP2 with either untagged PSmOrange (**Fig. 2a**) or with a vimentin-PSmOrange fusion protein (**Fig. 2b**). The initial and the photoconverted fluorescence signals of both PSFPs were spectrally well separated in the cells. Photoswitching of one PSFP did not cause substantial photobleaching of the other PSFP. Thus, using two spectrally compatible PSFPs, it is possible to simultaneously image four distinct intracellular populations.

To test the use of PSmOrange for studying intracellular dynamics together with common red fluorescent proteins, we next expressed PSmOrange–α-tubulin together with NLS-mCherry (**Fig. 2c**). A good spectral resolution between the orange and far-red forms of PSmOrange and red fluorescence of mCherry allowed using these two proteins simultaneously for multicolor imaging. As expected[24], the fast α-tubulin dynamics resulted in the complete replacement of the nonconverted orange PSmOrange–α-tubulin with the photoconverted far-red PSmOrange–α-tubulin, and vice versa, within 30 min after photoswitching.

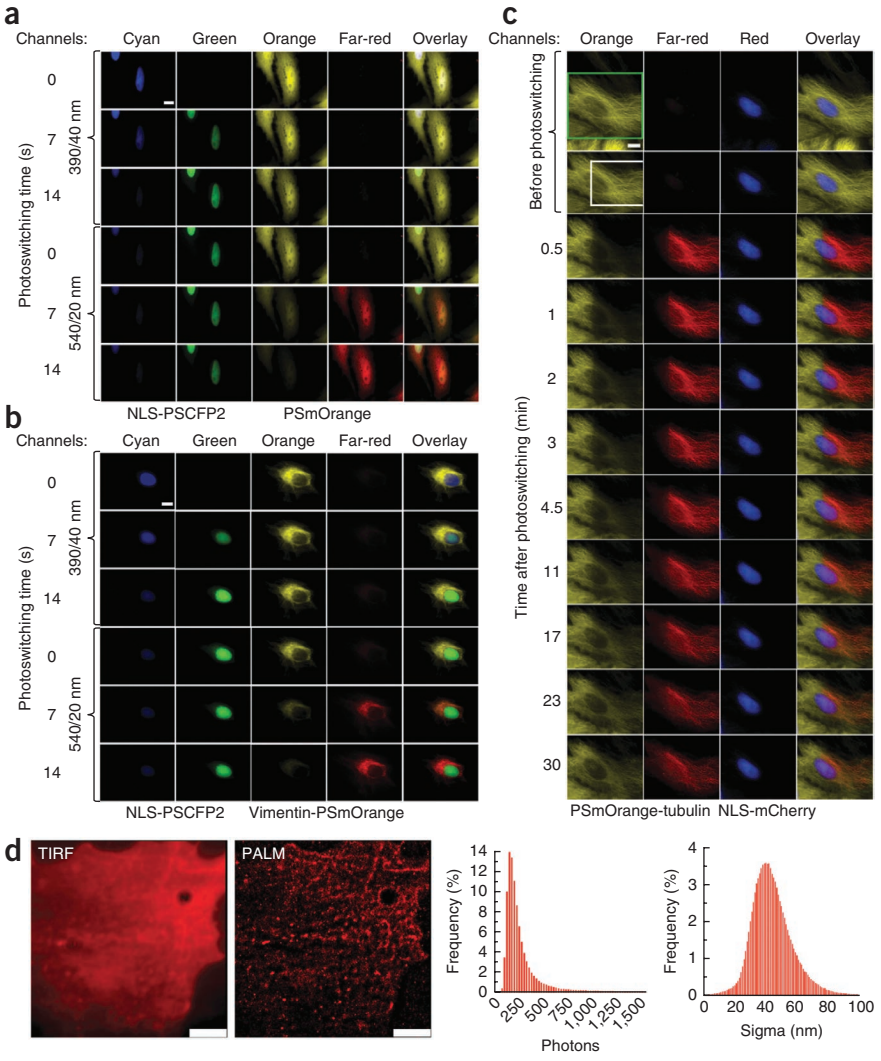

Figure 2 | Imaging of PSmOrange in mammalian cells. (**a**,**b**) Micrographs of HeLa cells expressing NLS-PSCFP2 in the nucleus with cytoplasmic PSmOrange (**a**) and vimentin-PSmOrange (**b**). Photoswitching of PSCFP2 and PSmOrange was performed with 390/40 nm and 540/20 nm light, respectively. (**c**) Micrographs show dynamics of PSmOrange-tubulin expressed together with NLS-mCherry in live HeLa cells. Photoswitching of PSmOrange was performed with 480/40 nm light for 60 s. The zoomed area is marked as a green box in the first row and is shown in all subsequent rows. The area of the PSmOrange photoconversion is indicated as a white box. Filter set information is available in Online Methods. Scale bars, 10 μm (**a**–**c**). (**d**) TIRF microscopy and a PALM images of EGFR-PSmOrange in fixed COS-7 cells. Scale bars, 5 μm. The histograms show distributions of photons and localization uncertainties. The mean number of photons is 337, and the mean molecular localization uncertainty (sigma) is 45 nm. Data are from 576,290 molecules collected from 5 cells.

Evaluation of PSmOrange as a PALM probe

We fused PSmOrange to epidermal growth factor receptor (EGFR), expressed the construct in COS-7 cells, and imaged the cells with PALM[11], using total internal reflection fluorescence (TIRF) illumination with 488-nm photoconversion and 640-nm excitation. The punctate distribution of the EGFR-PSmOrange chimera throughout the plasma membrane was similar to that seen previously[4] (**Fig. 2d**). The PALM images are notably more detailed when compared with the TIRF images. Photon statistics of the photoconverted far-red PSmOrange molecules showed that they have properties sufficient for PALM. Taken together, these tests indicate that PSmOrange can be used in PALM imaging. Furthermore, PSmOrange can be activated by blue rather than violet light, providing opportunities for PALM experiments on instruments lacking 405-nm lasers.

Imaging of PSmOrange in mouse models

To assess PSmOrange for use *in vivo*, we injected equal amounts of purified mKate2, mNeptune, E2-Crimson[16], TagRFP657, eqFP670 and photoswitched PSmOrange subcutaneously (~2 mm deep) into a mouse, as has been previously performed[25]. mKate2 and mNeptune exhibited the highest fluorescent signal in the 605/30 nm excitation channel (**Supplementary Fig. 8a**,**c**,**f**) whereas we detected photoconverted PSmOrange in both 605/30 nm and 640/30 nm channels, but PSmOrange exhibited several-fold higher fluorescence compared to far-red fluorescent proteins when excited using the 640/30 nm channel (**Supplementary Fig. 8b**,**d**,**g**). These data suggest that photoswitched PSmOrange could be used as a second far-red color complementary to mKate2 or mNeptune (**Supplementary Fig. 8e**), although the fluorescence of these proteins shows spectral overlap.

To explore how a deeper-tissue location could affect brightness of far-red fluorescent proteins and of photoswitched PSmOrange, we imaged the same amount of the purified proteins at 7.0 mm and 18.1 mm depth inside of a mouse phantom (**Supplementary Fig. 9**). The results were similar to those observed with subcutaneously injected fluorescent proteins (**Supplementary Fig. 8**). At both depths, photoconverted PSmOrange was brightest in the 640/30 nm excitation channel whereas mKate2 and mNeptune were brightest in the 605/30 nm channel (**Supplementary Fig. 9**).

To examine PSmOrange *in vivo*, we applied a test recently used to compare far-red fluorescent proteins in cells in mice[19]. HEK293T cells transiently expressing mKate2 or PSmOrange after photoconversion were injected intramuscularly into gluteal regions of a mouse. PSmOrange was detectable in two channels, 605/30 nm and 640/30 nm. mKate2 cells were brighter in 605/30 nm channel whereas PSmOrange cells were brighter in 640/30 nm channel (**Fig. 3a**,**b**).

To take advantage of the substantially lower *in vivo* absorbance of blue light compared to violet light[26], we tested the possibility of PSmOrange photoswitching directly in a mouse. We photoconverted a subcutaneously injected PSmOrange sample through the skin (**Supplementary Fig. 10**). The photoconverted far-red form of PSmOrange was clearly detectable in both 605/30 nm and 640/30 nm excitation channels. To test whether we can

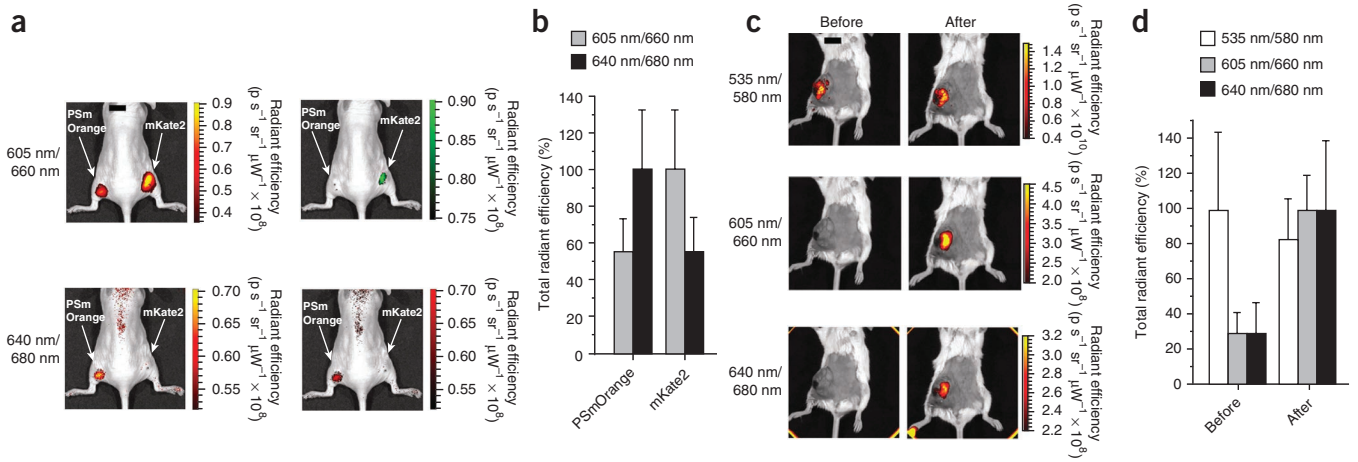

Figure 3 | Imaging of PSmOrange *in vivo*. (**a**) Whole body images of a mouse injected intramuscularly with 10^6 cells expressing mKate2 (right flank) or photoconverted PSmOrange (left flank). Images on the right are copies of images on the left but with fluorescence signals shown in green (605 nm excitation channel) and red (640 nm excitation channel) pseudocolors. (**b**) Total radiant efficiency corresponding to data in **a**. Total radiant efficiency of mKate2 was set as 100% in 605/30 nm excitation channel, and total radiant efficiency of PSmOrange was set as 100% in 640/30 nm excitation channel. Error bars, s.d. (n = 3). (**c**) Whole body images at the indicated excitation and emission wavelengths before and after photoconversion of PSmOrange in mammary tumor xenograft in a mouse. (**d**) Total radiant efficiency corresponding to data in **c**. Maximal total radiant efficiency in each channel was normalized to 100%. Error bars, s.d. (n = 4). In **a**–**d** the first and second numbers in 535 nm/580 nm, 605 nm/660 nm and 640 nm/680 nm indicate excitation and emission wavelengths, respectively. Scale bars (black, top of images in **a**,**c**), 1 cm.

photoconvert PSmOrange in cells inside mice, we grew MTLn3 adenocarcinoma cancer cells in mouse mammary gland. Before photoconversion, the PSmOrange-expressing tumor was only detectable in the 535/30 nm excitation channel (**Fig. 3c**,**d**). After the photoconversion using a 489-nm LED array, the tumor was clearly detected in the far-red 605/30 nm and 640/30 nm excitation channels.

PSmOrange far-red chromophore structure

To elucidate the chemical nature of the far-red chromophore of PSmOrange, we measured absorbance spectra of the denatured protein. The orange and far-red PSmOrange forms exhibited the same absorbance maxima at 387 nm after denaturation in acid and at 450 nm after denaturation in alkali. These peaks are characteristic of an *N*-acylimine–containing DsRed-like chromophore. Thus, both PSmOrange forms possibly contain an *N*-acylimine C=N group, which, similarly to the DsRed-like chromophore, is hydrated upon denaturation.

PSmOrange and mOrange polypeptides in the orange state did not exhibit polypeptide chain cleavage in SDS-PAGE after boiling (**Fig. 4a**). After photoswitching, however, we observed cleavage with formation of 19 kDa and 9 kDa fragments, suggesting that this cleavage may occur in the PSmOrange far-red chromophore. The PSmOrange far-red form was less stable with time than the orange form, with a half-life of 69 h (**Supplementary Fig. 11**). We then used mass spectrometry to analyze both forms of PSmOrange. The mass spectrum of PSmOrange chymotrypsin-digested fragments before photoswitching revealed a monoisotopic mass of 1211.39 Da, corresponding to the chromopeptide. The mass was as expected from the cyclization (loss of H_2O)

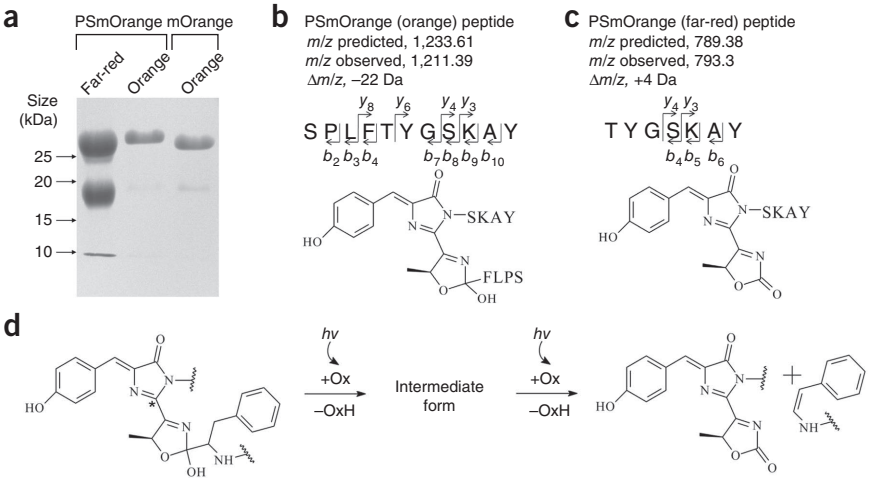

Figure 4 | Mass spectrometry analysis of the PSmOrange chromophore. (**a**) SDS-PAGE analysis of PSmOrange samples before and after photoswitching. (**b**,**c**) The chromophore-bearing peptides and structures of chromophores for PSmOrange before (**b**) and after (**c**) photoswitching. Calculated (first number) and observed (second number) m/z ratios for the orange-form peptide were: y_3, 381.21 and 381.21; y_4, 468.25 and 468.29; y_6, 696.38 and 696.32; y_8, 914.45 and 914.35; b_2, 185.09 and 185.13; b_3, 298.18 and 298.18; b_4, 445.24 and 445.26; b_7, 744.38 and 744.31; b_8, 831.41 and 831.42; b_9, 959.50 and 959.47; b_{10}, 1,030.54 and 1,030.45; and for the far-red–form peptide: y_3, 381.21 and 381.22; y_4, 468.25 and 468.26; b_4, 413.17 and 413.16; b_5, 541.27 and 541.23; b_6, 612.30 and 612.28. (**d**) Proposed scheme for the PSmOrange photoconversion. Asterisk indicates position 2 of the GFP-like chromophore core. Ox, oxidant molecule; OxH, reduced oxidant molecule; and *hv*, irradiation with blue-green light.

and double oxidation (loss of $2H_2$) of the chromophore inside the SPLFTYGSKAY fragment (cleavage after Leu60 and Tyr71). Tandem mass spectrometry (MS/MS) fragmentation showed that the dehydrogenation sites were located between the nitrogen and α-carbon of Thr65 and between Cα and Cβ atoms of Tyr66 (**Fig. 4b**). These data are consistent with the formation of two double bonds inside of the orange chromophore of PSmOrange, similar to the mOrange-like chromophore[27].

In the mass spectrum of photoswitched PSmOrange, we observed a new monoisotopic mass of 793.3 Da, 4 Da heavier than the theoretical mass of the TYGSKAY fragment. The mass increase suggested a modification of the chromopeptide that could result from cleavage between the dihydrooxazole ring and CH group in phenylalanine of the SPLFTYGSKAY fragment. MS/MS fragmentation of the TYGSKAY peptide (**Fig. 4c**) revealed that the far-red chromophore includes the C=N bond in the third dihydrooxazole ring of the mOrange-like chromophore, and that the new carbonyl group substitutes for the hydroxyl group in this ring (**Fig. 4d**). The observed cleavage of the PSmOrange far-red form in SDS-PAGE is consistent with the suggested far-red chromophore structure based on mass spectrometry.

DISCUSSION

PSmOrange has spectral advantages over conventional green-to-red PSFPs. First, PSmOrange is red-shifted, enabling its use for simultaneous multicolor imaging with green and blue fluorescent proteins and PSCFP2. Second, the orange and far-red forms of PSmOrange and mCherry can be spectrally separated, so that it is also possible to use PSmOrange simultaneously with red fluorescent proteins and PAFPs. Third, when excited using standard red laser lines or red-shifted excitation filters, photoconverted PSmOrange is brighter than conventional far-red fluorescent proteins (**Fig. 3a** and **Supplementary Figs. 5**, **8** and **9**).

Chromophore structures of most fluorescent proteins with a tyrosine residue in the chromophore-forming tripeptide include the 4-(p-hydroxybenzylidene)-5-imidazolone heterocyclic core, which is the GFP-like chromophore[28]. The C=N substituent transforms the GFP-like chromophore into the mOrange-like chromophore, exhibiting a red shift of ~35–55 nm. The C=O group-substituent leads to a red shift of ~80–100 nm that is observed in the red fluorescent protein from *Anemonia sulcata* (asFP595)[29]. An *N*-acylimine group, which consists of two double bonds (C=N–C=O), transforms the GFP-like chromophore into the DsRed-like chromophore. The *N*-acylimine should provide a bathochromic shift substantially larger than that of single C=N or C=O groups, but this is not the case when compared to the C=O substituent. The reason is that in all crystal structures of fluorescent proteins with the DsRed-like chromophore the C=O group is out of the chromophore plane[27]. This means its conjugation with the chromophore core and hence the red-shift are substantially reduced.

Mass-spectrometry data indicate that the far-red PSmOrange chromophore contains an *N*-acylimine substituent in the GFP-like core. Its C=N bond is involved in the five-member dihydrooxazole ring, which is characteristic of the mOrange-like chromophore. Light-induced oxidation causes polypeptide chain cleavage and formation of a C=O group linked to the five-member ring. Thus, the involvement of the *N*-acylimine functionality in the dihydrooxazole ring results in all its bonds being in the chromophore plane and hence in a more efficient conjugation of the C=O group, as compared to the DsRed-like chromophore.

Using the resolved structures of the orange and far-red chromophores, we can suggest a chemical scheme of PSmOrange photoswitching (**Fig. 4d**). As photoswitching accelerates in the presence of oxidant and requires two photons of blue-green light, the orange to far-red transformation should include two steps of a photo-oxidative polypeptide cleavage. A hydroxyl group of the orange chromophore is transformed into a carbonyl group of the far-red chromophore. We suggest that this reaction is similar to a two-step oxidation of a hydroxyl group of alcohols to a carbonyl group of aldehydes and ketones in the presence of oxidants[30].

METHODS

Methods and any associated references are available in the online version of the paper at http://www.nature.com/naturemethods/.

Accession codes. GenBank: JN376081 (*PSmOrange*).

Note: Supplementary information is available on the Nature Methods website.

ACKNOWLEDGMENTS

We thank J. Zhang and L. Tesfa for assistance with flow cytometry, H. Xiao for help with mass-spectrometry analysis, K. Kim and G. Filonov for assistance with mouse experiments and useful discussions, M. Davidson (Florida State University) for vimentin, keratin, myosin and paxillin plasmids, and B. Glick (University of Chicago), D. Chudakov and K. Lukyanov (both from Institute of Bioorganic Chemistry) for plasmids encoding far-red fluorescent proteins. This work was supported by US National Institutes of Health (GM073913 to V.V.V. and CA100324 to J.C.) and by the National Institutes of Health Intramural Research Program including the National Institute of Biomedical Imaging and Bioengineering (to G.H.P.).

AUTHOR CONTRIBUTIONS

O.M.S. developed the protein and characterized it *in vitro*. O.M.S. and G.H.P. characterized the protein in mammalian cells. O.M.S. and L.-M.T. characterized the protein in mouse models. O.M.S., Y.W. and J.S.C. performed tumor experiments. V.V.V. designed the project and, together with O.M.S., planned and discussed the project, and wrote the manuscript.

COMPETING FINANCIAL INTERESTS

The authors declare no competing financial interests.

Published online at http://www.nature.com/naturemethods/.
Reprints and permissions information is available online at http://www.nature.com/reprints/index.html.

1. Lukyanov, K.A., Chudakov, D.M., Lukyanov, S. & Verkhusha, V.V. Innovation: photoactivatable fluorescent proteins. *Nat. Rev. Mol. Cell Biol.* **6**, 885–891 (2005).
2. Patterson, G.H. & Lippincott-Schwartz, J. A photoactivatable GFP for selective photolabeling of proteins and cells. *Science* **297**, 1873–1877 (2002).
3. Subach, F.V. *et al.* Photoactivatable mCherry for high-resolution two-color fluorescence microscopy. *Nat. Methods* **6**, 153–159 (2009).
4. Subach, F.V. *et al.* Bright monomeric photoactivatable red fluorescent protein for two-color super-resolution sptPALM of live cells. *J. Am. Chem. Soc.* **132**, 6481–6491 (2010).
5. Chudakov, D.M., Lukyanov, S. & Lukyanov, K.A. Tracking intracellular protein movements using photoswitchable fluorescent proteins PS-CFP2 and Dendra2. *Nat. Protoc.* **2**, 2024–2032 (2007).
6. McKinney, S.A. *et al.* A bright and photostable photoconvertible fluorescent protein. *Nat. Methods* **6**, 131–133 (2009).
7. Ando, R., Hama, H., Yamamoto-Hino, M., Mizuno, H. & Miyawaki, A. An optical marker based on the UV-induced green-to-red photoconversion of a fluorescent protein. *Proc. Natl. Acad. Sci. USA* **99**, 12651–12656 (2002).

8. Habuchi, S., Tsutsui, H., Kochaniak, A.B., Miyawaki, A. & van Oijen, A.M. mKikGR, a monomeric photoswitchable fluorescent protein. *PLoS ONE* **3**, e3944 (2008).
9. Hoi, H. *et al.* A monomeric photoconvertible fluorescent protein for imaging of dynamic protein localization. *J. Mol. Biol.* **401**, 776–791 (2010).
10. Toomre, D. & Bewersdorf, J. A new wave of cellular imaging. *Annu. Rev. Cell Dev. Biol.* **26**, 285–314 (2010).
11. Stiel, A.C. *et al.* Generation of monomeric reversibly switchable red fluorescent proteins for far-field fluorescence nanoscopy. *Biophys. J.* **95**, 2989–2997 (2008).
12. Folling, J. *et al.* Fluorescence nanoscopy by ground-state depletion and single-molecule return. *Nat. Methods* **5**, 943–945 (2008).
13. Lim, Y.T. *et al.* Selection of quantum dot wavelengths for biomedical assays and imaging. *Mol. Imaging* **2**, 50–64 (2003).
14. Deliolanis, N.C. *et al.* Performance of the red-shifted fluorescent proteins in deep tissue molecular imaging applications. *J. Biomed. Opt.* **13**, 044008 (2008).
15. Morozova, K.S. *et al.* Far-red fluorescent protein excitable with red lasers for flow cytometry and superresolution STED nanoscory. *Biophys. J.* **99**, L13–L15 (2010).
16. Strack, R.L. *et al.* A rapidly maturing far-red derivative of DsRed-Express2 for whole-cell labeling. *Biochemistry* **48**, 8279–8281 (2009).
17. Shcherbo, D. *et al.* Far-red fluorescent tags for protein imaging in living tissues. *Biochem. J.* **418**, 567–574 (2009).
18. Lin, M.Z. *et al.* Autofluorescent proteins with excitation in the optical window for intravital imaging in mammals. *Chem. Biol.* **16**, 1169–1179 (2009).
19. Shcherbo, D. *et al.* Near-infrared fluorescent proteins. *Nat. Methods* **7**, 827–829 (2010).
20. Kremers, G.J., Hazelwood, K.L., Murphy, C.S., Davidson, M.W. & Piston, D.W. Photoconversion in orange and red fluorescent proteins. *Nat. Methods* **6**, 355–358 (2009).
21. Bogdanov, A.M. *et al.* Green fluorescent proteins are light-induced electron donors. *Nat. Chem. Biol.* **5**, 459–461 (2009).
22. Shaner, N.C. *et al.* Improving the photostability of bright monomeric orange and red fluorescent proteins. *Nat. Methods* **5**, 545–551 (2008).
23. Strack, R.L. *et al.* A non-cytotoxic DsRed variant for whole-cell labeling. *Nat. Methods* **5**, 955–957 (2008).
24. Etienne-Manneville, S. From signaling pathways to microtubule dynamics: the key players. *Curr. Opin. Cell Biol.* **22**, 104–111 (2010).
25. Kuo, C., Coquoz, O., Troy, T.L., Xu, H. & Rice, B.W. Three-dimensional reconstruction of *in vivo* bioluminescent sources based on multispectral imaging. *J. Biomed. Opt.* **12**, 024007 (2007).
26. Smith, A.M., Mancini, M.C. & Nie, S. Bioimaging: second window for *in vivo* imaging. *Nat. Nanotechnol.* **4**, 710–711 (2009).
27. Shu, X., Shaner, N.C., Yarbrough, C.A., Tsien, R.Y. & Remington, S.J. Novel chromophores and buried charges control color in mFruits. *Biochemistry* **45**, 9639–9647 (2006).
28. Ormö, M. *et al.* Crystal structure of the *Aequorea victoria* green fluorescent protein. *Science* **273**, 1392–1395 (1996).
29. Yampolsky, I.V. *et al.* Synthesis and properties of the chromophore of the asFP595 chromoprotein from *Anemonia sulcata*. *Biochemistry* **44**, 5788–5793 (2005).
30. Tojo, G. & Fernández, M. *Oxidation of Alcohols to Aldehydes and Ketones* (Springer, New York, 2006).

ONLINE METHODS

Mutagenesis and screening of libraries. We PCR-amplified an *mOrange*[31] gene as a BglII-EcoRI fragment (**Supplementary Table 2**) and inserted it into a pBAD/His-B vector (Invitrogen). A site-specific mutagenesis of the *mOrange* gene was performed using a QuickChange Mutagensis kit (Stratagene). For simultaneous mutagenesis at several positions, we applied an overlap-extension approach[32]. A random mutagenesis was performed using a GeneMorph II Random Mutagenesis kit (Stratagene) or a Diversity PCR Random Mutagenesis kit (Clontech) under conditions resulting in a mutation frequency of up to 16 mutations per 1,000 base pairs. After mutagenesis we electroporated a mixture of the mutated genes into LMG194 bacterial host cells (Invitrogen).

Libraries of 10^7–10^8 independent clones of the mOrange mutants were photoswitched with a custom built 489 nm LED array (adjusted to 93 mW cm^{-2}) and screened using a MoFlo (Dako) FACS followed by colony visualization, using a Leica MZ16F fluorescence stereomicroscope, as previously described[3]. After each round of FACS screening, typically 10–20 best photoswitchable candidate clones were sequenced, purified and characterized before the next round of mutagenesis.

cDNA for the final variant, PSmOrange, is available upon request.

Characterization of purified proteins. We expressed mOrange[31], mOrange2 (ref. 22) (contained Q63H and F100Y mutations comparing to mOrange), mNeptune[18] and PSmOrange mutant proteins with polyhistidine tags in LMG194 bacteria grown in a minimal medium (RM) supplemented with 0.002% arabinose for 24–48 h at 37 °C and then purified using a Ni-NTA agarose (Qiagen). For spectroscopy, photoswitching of purified proteins was performed with the 489 nm LED array (adjusted to 280 mW cm^{-2}) in 1.5 ml transparent Eppendorf tube on ice. Excitation and emission spectra of recombinant proteins were measured with a FluoroMax-3 spectrofluorometer (Jobin Yvon). For absorbance measurements, a Hitachi U-3010 spectrophotometer was used.

To determine extinction coefficients of orange forms, we measured the mature chromophore concentration, as previously described for mOrange[31]. For this, the purified mOrange and PSmOrange proteins were alkali-denatured. The extinction coefficient of the GFP-like chromophore is 44,000 M^{-1} cm^{-1} at 447 nm in 1 M NaOH[33]. Based on the absorbance of the native and denatured proteins, molar extinction coefficients for the native states were calculated. To determine extinction coefficients of far-red forms, we photoswitched purified proteins with the 489 nm LED array (adjusted to 280 mW cm^{-2}) for 10 min on ice in the presence of 5 mM $K_3Fe(CN)_6$. With this oxidant concentration, the maximally achievable far-red fluorescence was not dependent on the 489-nm light intensity. Extinction coefficients were calculated based on a comparison between the absorbance decrease of orange forms (at 548 nm and 546 nm for PSmOrange and mOrange, respectively) and the absorbance increase of far-red forms (at 634 nm and 631 nm for PSmOrange and mOrange, respectively). To determine quantum yields, we compared the fluorescence intensities of orange and far-red forms at pH 8.5 to the fluorescence intensities of equally absorbing amounts of mOrange in the orange form (quantum yield is 0.69; ref. 31) and mNeptune (quantum yield is 0.2; ref. 18). Equilibrium pH titrations were performed using a series of buffers (100 mM NaOAc, 300 mM NaCl for pH 2.5–5.0 and 100 mM NaH_2PO_4, 300 mM NaCl for pH 4.5–10.0).

We measured photobleaching kinetics using purified proteins in PBS (pH 7.4) at 1 mg ml^{-1} in aqueous drops in oil using Olympus IX81 inverted microscope equipped with a 200 W metal halide arc lamp (Prior), a 100× 1.4 numerical aperture (NA) oil-immersion objective lens (UPlanSApo, Olympus), 540/20 nm excitation and 575/30 nm emission filters for orange forms, and 605/40 nm excitation and 640LP nm emission filters for far-red forms. The microscope was operated with SlideBook 4.2 software (Intelligent Imaging Innovations). Light power densities were measured at a rear focal plane of the objective lens, and light power at the sample was estimated. We measured photobleaching kinetics using the above conditions with a 480/40 nm filter for photoswitching. The data were normalized to a spectral output of the lamp, transmission profiles of the filters and dichroic mirror, and absorbance spectra of the respective proteins.

To study protein maturation, LMG194 bacteria transformed with *mOrange* or *PSmOrange* genes were grown in an RM medium supplemented with ampicillin (100 μg ml^{-1}) at 37 °C overnight. The next morning, we diluted bacterial cells to optical density 1.0 at 600 nm and added 0.2% arabinose. Upon induction of protein expression, bacterial cultures were grown at 37 °C in 50-ml tubes filled to the brim and tightly sealed to restrict oxygen supply. After 2 h, the cultures were centrifuged in the same tightly closed tubes. After opening the tubes, we purified the proteins using the Ni-NTA resin within 30 min, with all procedures and buffers at or below 4 °C. Protein maturation occurred in PBS at 37 °C. Orange fluorescence signal of the proteins was monitored using the FluoroMax-3 spectrofluorometer.

Mammalian plasmids and cell culture. To construct pPSmOrange-C1, pPSmOrange-α-Tubulin and pPSmOrange-Myosin plasmids, the *PSmOrange* gene was swapped with the *EGFP* gene or the *mTagBFP* gene in the pEGFP-C1, pEGFP-α-Tubulin and pmTagBFP-Myosin vectors (Clontech), respectively. To design a pH2B-PSmOrange plasmid, the *PSmOrange* gene was swapped with the *PAmCherry1* gene in the pH2B-PAmCherry1 plasmid[3]. To construct pVimentin-PSmOrange, pKeratin-PSmOrange and pPaxillin-PSmOrange plasmids, the *PSmOrange* gene was swapped with the *mTagBFP* gene in the pVimentin-mTagBFP, pKeratin-mTagBFP and pPaxillin-mTagBFP vectors, respectively. To construct a pPSmOrange-N1 plasmid, the *PSmOrange* gene was PCR amplified as an AgeI-NotI fragment and swapped with the *EGFP* gene in a pEGFP-N1 vector (Clontech). To generate pNLS-PSCFP2 plasmid, AgeI-NotI fragment containing the *PSCFP2* gene was cut out from the pPSCFP2-N1 plasmids and was swapped with the *ECFP* gene in a pNLS-ECFP plasmid. To construct a pEGFR-PSmOrange plasmid, a SacII-BsrGI fragment containing the PSmOrange gene was PCR-amplified and swapped with the *mRFP1* gene in the pEGFR-mRFP1 plasmid[34].

HeLa and COS-7 cells were grown in a Dulbecco's Modified Eagle Medium (DMEM) containing 10% FBS and 2 mM glutamine (all from Invitrogen). MTLn3 cells were grown in alpha-modified Eagle medium containing 5% FBS and 2 mM glutamine (all from Invitrogen). Cells were grown in #1.5 glass-bottom culture dishes (MatTek Corporation). Plasmid transfections were performed either with an Effectene (Qiagen) or a FuGENE (Roche) reagents. Live HeLa cells were photoswitched and imaged in a dye-free

doi:10.1038/nmeth.1664

DMEM medium without serum (Invitrogen). COS-7 cells were incubated at 37 °C for 36 h before fixing with 4% paraformaldehyde (Electron Microscopy Sciences).

Imaging of mammalian cells. Wide-field epifluorescence imaging of live mammalian cells was performed 48–72 h after transfection. Cells were imaged using the Olympus IX81 inverted microscope described above. A 480/40 nm (1,050 W cm^{-2}, here and below the light intensities are estimated at the sample) or 540/20 nm (1,130 W cm^{-2}) filters were used for photoswitching PSmOrange, and a 390/40 nm filter (900 W cm^{-2}) was used for photoswitching PSCFP2. The 540/20 nm excitation and 575/30 nm emission filters (126–468 W cm^{-2}) were used to image orange forms, and the 605/40 nm excitation in combination with 640LP nm emission filters (360 W cm^{-2}) or 622/36 nm excitation in combination with 680LP emission filters (340 W cm^{-2}) to image far-red forms. The 390/40 nm excitation and 460/40 nm emission filters (360 W cm^{-2}) were used to image the cyan form of PSCFP2, and the 480/40 nm excitation and 530/40 nm emission filters (432 W cm^{-2}) were used to image the green form of PSCFP2. The 570/30 nm excitation and 615/40 nm emission filters (120 W cm^{-2}) were used to image mCherry. All filter sets were from Chroma.

PALM imaging of single molecules was performed on an Olympus IX71 microscope using a 60× 1.45 NA PlanApoN TIRF objective (Olympus), as previously described[35,36]. The lasers were a 100 mW 640 nm (Coherent) and a 50 mW 488 nm (Oxxius). Photoswitched EGFR-PSmOrange single molecules were imaged using 640-nm laser light. Data were collected in 100-ms frames over 12,000 frames with a pulse of 488 nm laser light every 10 frames. Power levels measured near the rear aperture of the objective lens were <2 mW (estimated <80 W cm^{-2} at the sample) for the 640-nm laser and ranged from ~65 µW to ~8 mW (estimated 2.6–320 W cm^{-2} at the sample) for the 488-nm laser. The dichroic mirror was designed for use with four laser lines (Di01-R405/488/561/635-25x36, Semrock) and fluorescence was detected through a long-pass far-red filter (BLP01-635R-25, Semrock) with an iXon electron-multiplying charge-coupled device (EMCCD) camera (Andor Technology). Image analysis was performed as previously described[35]. Coverslips were cleaned with piranha wash as previously described[37]. Fiduciary markers were 25 nm gold nanorodz (Nanopartz). The fluorescence was collected during the 12,000 frames for a diffraction-limited TIRF image. The position and uncertainty from 183,089 molecules were plotted as Gaussian-normalized spots to form a PALM image.

Imaging of purified proteins in mouse models. Bacterial plasmids encoding several far-red fluorescent proteins were kindly provided by B. Glick (University of Chicago) and D. Chudakov and K. Lukyanov (both from Institute of Bioorganic Chemistry). We expressed and purified recombinant mKate2, mNeptune, E2-Crimson, TagRFP657 and eqFP670 proteins as described above for PSmOrange. The purified fluorescent proteins were diluted in PBS to the equal concentrations calculated based on the extinction coefficients at the chromophore absorbance maxima. All procedures with mice were conducted in accordance with US National Institutes of Health regulations, and approved by the Albert Einstein College of Medicine Animal Use Committee. Albino C57BL/6 6-8 weeks old female mice (Jackson Laboratory) were used. Isoflurane (Aerrane) was used to sedate the mice during short imaging sessions. Belly fur was removed using a depilatory cream, and 10 µl volume of each fluorescent protein (100 µM) was injected subcutaneously into mice. Imaging of mice was performed at 37 °C using an IVIS Spectrum instrument in the epifluorescence mode (Caliper Life Sciences). The fluorescent signals of different far-red fluorescent proteins and photoswitched PSmOrange were compared as total radiant efficiencies. A radiant efficiency is equal to the radiance of the object divided by the illumination intensity. When region of interest (ROI) measurements were made, a total radiant efficiency within the ROI is the efficiency per pixel integrated over the ROI area, so the resulting units of the total radiant efficiency is area or square centimeters.

To image fluorescent proteins in the XFM-2 rubber phantom mouse (Caliper Life Sciences), we placed 5 µl volume of each fluorescent protein (16 µM) 15 mm deep inside into a bore of the phantom. The bores were located at 7.0 mm and 18.1 mm distance from the imaging surface. Images were taken in different combinations of the far-red excitation and emission channels using an epifluorescence mode of the IVIS Spectrum instrument. A signal-to-background ratio was calculated for each wavelength combination for each fluorescent protein, using the phantom mouse without protein sample inside as a background reference. All quantitative measurements of fluorescence signal were performed using the Living Image Software 4.0 (Caliper Life Sciences).

Imaging of cells in live mice. HEK293T cells expressing PSmOrange were illuminated with a 489-nm LED array (adjusted to 200 mW cm^{-2}) in PBS. We injected 10^6 HEK293T cells expressing either mKate2 or photoconverted PSmOrange in 50 µl of 1:1 mixture of F12 medium and matrigel (BD Biosciences) intramuscularly into the right and left gluteal musculature of nude (Nu:Nu) mice (Charles River, Strain 088). Imaging was performed ~20 min after the injection using an IVIS Spectrum instrument in the epifluorescence mode.

To prepare mammary tumors in mice, we used female 5- to 6-week-old BALB/c severe combined immunodeficient (SCID/Ncr) mice. They were purchased from the US National Cancer Institute and housed in a pathogen-free barrier facility until use. Mice were injected with 10^6 MTLn3 cells in the mammary gland. The tumor surface fur was removed using a depilatory cream. Several-week-old tumors were illuminated with 489 nm LED array (adjusted to 200 mW cm^{-2}). To avoid overheating the mouse, the skin in the illumination area was cooled using hand-made optically transparent cooler with flowing water. Twenty-four hours before illumination, 500 µl of 5 mM $K_3Fe(CN)_6$ was injected subcutaneously around the tumor. Imaging of tumor was performed using an IVIS Spectrum instrument in the epifluorescence mode.

Mass spectrometry analysis. To run reducing SDS-PAGE, we incubated 10 µl (1 mg ml^{-1}) proteins samples at 95 °C in an electrophoresis sample buffer for 5 min before application to a 15% polyacrylamide gel.

An aliquot of 50 µg of 6His-tagged PSmOrange was denatured by heating in 15 µl of 4.8 M guanidine chloride at 80 °C for 3 min. Then the sample was cooled to room temperature. 30 µl of

2× chymotrypsin buffer containing 0.2 M Tris-HCl (pH 7.8) and 20 mM $CaCl_2$ as well as 15 µl of water were added, and then chymotrypsin was added at an enzyme:protein ratio of 1:60. The digests were incubated at room temperature (24 °C) for 22 h and quenched with 0.1% trifluoroacetic acid (TFA). We applied the digestion product to a reverse-phase high-performance liquid chromatography (HPLC) chromatography (Agilent Technologies). The peptides were eluted by a linear gradient of acetonitrile in the same buffer. The effluent was monitored by an absorbance at 210 nm to detect peptide bonds and at 348 nm to detect denatured chromophore-containing peptides.

The chymotryptic peptides were mixed (1:1) with α-cyano-4-hydroxycinnamic acid solution (50% acetonitrile and water containing 0.1% tri-fluoroacetic acid). An aliquot of 1 µl of the mixture was put on a Matrix-assisted laser desorption/ionization (MALDI) target and air-dried. Mass spectra were acquired on a 4800 MALDI time of flight (TOF)/TOF mass spectrometer (Applied Biosystems). The instrument was equipped with a Nd:YAG laser (PowerChip, JDS Uniphase) operating at 200 Hz and controlled by Applied Biosystems 4000 Series Explorer version 3.6 software. Each spectrum was accumulated with 500 shots in a positive ion mode. MS/MS were acquired in a PSD mode with mass isolation window of ±3 Da.

31. Shaner, N.C. *et al.* Improved monomeric red, orange and yellow fluorescent proteins derived from *Discosoma* sp. red fluorescent protein. *Nat. Biotechnol.* **22**, 1567–1572 (2004).
32. Ho, S.N., Hunt, H.D., Horton, R.M., Pullen, J.K. & Pease, L.R. Site-directed mutagenesis by overlap extension using the polymerase chain reaction. *Gene* **77**, 51–59 (1989).
33. Chudakov, D.M. *et al.* Photoswitchable cyan fluorescent protein for protein tracking. *Nat. Biotechnol.* **22**, 1435–1439 (2004).
34. Verkhusha, V.V. & Sorkin, A. Conversion of the monomeric red fluorescent protein into a photoactivatable probe. *Chem. Biol.* **12**, 279–285 (2005).
35. Betzig, E. *et al.* Imaging intracellular fluorescent proteins at nanometer resolution. *Science* **313**, 1642–1645 (2006).
36. Manley, S. *et al.* High-density mapping of single-molecule trajectories with photoactivated localization microscopy. *Nat. Methods* **5**, 155–157 (2008).
37. Shroff, H. *et al.* Dual-color superresolution imaging of genetically expressed probes within individual adhesion complexes. *Proc. Natl. Acad. Sci. USA* **104**, 20308–20313 (2007).

doi:10.1038/nmeth.1664